ADVANCED ENERGY & SUSTAINABILITY RESEARCH Open Access
www.advenergysustres.com

26999412, 0, Downloaded from https://onlinelibrary.wiley.com/doi/10.1002/aesr.202200141 by Technical University Eindhoven, Wiley Online Library on [16/02/2023]. See the Terms and Conditions (https://onlinelibrary.wiley.com/terms-and-conditions) on Wiley Online Library for rules of use; OA articles are governed by the applicable Creative Commons License

Increased Photoelectrochemical Performance of Vanadium Oxide Thin Film by Helium Plasma Treatment with Auxiliary Molybdenum Deposition

Shin Kajita, Tomoki Eda, Shuangyuan Feng, Hirohiko Tanaka, Anja Bieberle-Hütter, and Noriyasu Ohno*

Helium (He) plasma treatment can be a versatile tool to fabricate nanostructures on a surface and change the surface chemistry. Herein, vanadium (V) thin film is exposed to helium plasmas and the changes in morphology and surface properties are investigated. The irradiation condition at which the surface morphology can be changed is identified. During the He plasma irradiation, molybdenum (Mo) from the sample cover deposits and formation of composite nanostructured photoelectrode with a combination of V_2O_5/MoO_3 occurs. The photoelectrochemical (PEC) performance increases threefold through the plasma treatment. In addition to the increase in the surface area, the formation of the heterogenous/composite structure, oxygen vacancies, and reduced oxides such as V_6O_{13} decreases the charge-transfer resistance and contributes to the improvement in the PEC performance.

1. Introduction

Vanadium (V) oxides and their composites are regarded as promising materials for a variety of applications such as lithium-ion batteries,[1] pseudocapacitors,[2] fuel cells,[3] photocatalysts,[4,5] and gas sensors.[6] This is due to their good catalytic activity, suitable intercalation/deintercalation, and strong electron–electron correlation.[7,8] Various processing methods have been used to fabricate vanadium oxide thin films and nanostructures. For example, pulsed laser deposition (PLD),[9] magnetron sputtering,[10] chemical vapor deposition (CVD),[11] plasma-enhanced CVD,[12] sol–gel method,[13,14] and sol–gel dip coating[15] were used to deposit thin films; hydrothermal process,[16] thermal pyrolysis,[17] electrospinning,[18] ion beam sputtering,[19] and helium (He) plasma treatment[5] were used for nanostructuring.

Among these methods, He plasma treatment is a novel method, which forms fiberform nanostructures (FNs) called fuzz on various metals including tungsten, molybdenum, rhenium, rhodium, tantalum, platinum, niobium, and V.[5,20–25] The process is a bottom-up process accompanied by the growth of He bubbles on the top surface layer (thickness of 100–200 nm) and the formation and diffusion of adatoms.[26–30] Application of oxidized fuzz has been studied including the application of tungsten trioxides (WO_3) as gas sensors[31–36] WO_3, iron oxides,[37,38] titania,[39,40] and V oxides[5] as photoelectrodes. On the fuzzy oxides, in addition to the increase in the active area to be used for reactions,[38] other positive aspects of the He treatment have been revealed, such as the formation of oxygen vacancies,[36] which can improve photoelectrochemical (PEC) performance, and stabilization of the anatase structure of titania.[40] Zaho et al. found that good tailoring of the amount of oxygen vacancies is needed to achieve the highest performance in WO_3 photoelectrodes.[41]

Growth of FNs by He plasma treatment was also demonstrated on bulk V samples;[5,22] however, the fabrication was not tested on thin films yet. Regarding practical applications, such as photoelectrodes or gas sensors, it is important to investigate thin films. However, the growth rate and growth condition achieved by He plasma treatment on thin films can differ from those on bulk material.[37,42] For example, on 100 nm thick W thin films, nonuniform island structures were formed, and the growth rate of the fuzzy layer was faster than that on bulk W.[43] Therefore, it is important to explore the effects of He plasma treatment on thin films in addition to bulk samples.

S. Kajita
Graduate School of Frontier Sciences
The University of Tokyo
5-1-5 Kashiwanoha, Kashiwa, Chiba 277-8561, Japan
E-mail: kajita@k.u-tokyo.ac.jp

S. Kajita, T. Eda, H. Tanaka, N. Ohno
Graduate School of Enginnering
Nagoya University
Nagoya 464-8603, Japan

S. Feng
National Institute for Fusion Science
National Institutes of Natural Sciences
Toki, Gifu 509-5292, Japan

A. Bieberle-Hütter
Dutch Institute for Fundamental Energy Research (DIFFER)
P.O. Box 6336, 5600 HH Eindhoven, The Netherlands

The ORCID identification number(s) for the author(s) of this article can be found under https://doi.org/10.1002/aesr.202200141.

© 2023 The Authors. Advanced Energy and Sustainability Research published by Wiley-VCH GmbH. This is an open access article under the terms of the Creative Commons Attribution License, which permits use, distribution and reproduction in any medium, provided the original work is properly cited.

DOI: 10.1002/aesr.202200141

 © 2023 The Authors. Advanced Energy and Sustainability Research published by Wiley-VCH GmbH

Concerning the photocatalytic and PEC application, a drawback of metal oxides semiconductor is the low performance due to the high recombination rate of photoinduced electron-hole pairs. Several methods are being investigated to improve the performance[44]: morphology control, defect engineering including oxygen sub-stoichiometry,[45] doping with different elements,[46] formation of heterogeneous junction using multilayered or composite materials.[47,48] For vanadium oxides, Shen et al. fabricated various vanadium oxides by hydrothermal synthesis and measured the photocatalytic and PEC properties.[16] All vanadium oxides (V_2O_5, V_6O_{13}, and two polymorphs of VO_2) were qualified as visible-light-responsive photocatalysts for water-splitting (hydrogen production) with lower bandgap energies than that of TiO_2. One of the strategies taken to improve the performance of vanadium oxides is a mixture with other semiconductors including bismuth vanadate ($BiVO_4$)[49,50] and molybdenum trioxide (MoO_3).[51–53] Arunachalam et al. showed that the incident photon to current efficiency improved more than 50% at the wavelength of 425 nm by forming a heterostructure of $V_2O_5/BiVO_4$,[49] and Chuai et al. showed that V_2O_5/MoO_3 composite exhibited enhanced visible-light photocatalytic activity because of the formation of heterostructures at the interface between V_2O_5 and MoO_3.[51]

In this study, we performed He plasma treatment on V thin films as electrode material of PEC water-splitting. During the irradiation, auxiliary Mo deposition from the sample holder occurred and formed V and Mo composite, while forming fuzzy structures on the surface. The PEC measurements show that the PEC performance increased 2.8 times by plasma treatment. The mechanism of the enhanced PEC performance is discussed in a combination of chemical, structural, and electrochemical analyses. It is shown that plasma treatment contributes to changes of surface chemistry in addition to morphology change.

2. Morphology

Helium plasma irradiation of V thin films was performed at various incident ion energy, E_i, and surface temperature, T_s, in the ranges of $52 \leq E_i \leq 98$ eV and $870 \leq T_s \leq 1120$ K. The exposure time was 1 h and the He fluence was in the range of $3.7 - 16 \times 10^{25}$ m^{-2}. The variation of the He fluence was caused by variation of the He flux, which was changed to control T_s, since thermal contact resistance with the sample holder varies with each irradiation. As will be shown later, although the fluence is slightly different, this should not impact the nanostructure formation because it is important whether the fluence exceeds a certain threshold. **Figure 1**a,b shows SEM micrographs of a V thin film exposed at E_i of 70 eV and T_s of 970 K at two magnifications. It can be seen that fuzz grows on the surface. In Figure 1a,b, the He fluence is 5.4×10^{25}m^{-2}, which is the lowest fluence among the three samples. Helium fluence dependence of fuzz growth on W has been well investigated.[54] There is a minimum threshold called incubation fluence to initiate the fuzz growth, and the thickness of the fuzzy layer increases in proportion to the square root of the He fluence. On analogy with the fuzz growth on W, Figure 1a,b suggests that the following irradiation experiments satisfy the necessary condition regarding the He fluence. Figure 1c–f shows SEM micrographs of V thin films exposed at higher temperatures of 1080 and 1120 K and at E_i of 70 and 95 eV, respectively. On both samples, fuzz cannot be seen, although a rough surface is formed. In Figure 1c,d, fiber-form structures develop forming a partial nanofuzz structure. Only a rough microstructure is identified in Figure 1e,f. In this study, we categorize the morphology changes seen in Figure 1 as fuzz, partially fuzz, and roughened. When fuzz is formed under the conditions used in this study, the thickness of the fuzzy layer was 1 μm (Figure S1 and S2, Supporting Information).

Figure 2 represents the relationship between the morphology changes and the irradiation conditions (T_s and E_i). When T_s is in the range of 850–1000 K, fuzz grows on the surface independent of the incident ion energy. When $T_s > 1050$ K and $E_i < 90$ eV, as shown in Figure 1b, the FNs are only partially seen on the surface (partially fuzz). At $T_s > 1050$ K and $E_i > 90$ eV, rough structures without fuzz cover the surface, as shown in Figure 1. It is known that in the temperature range for fuzz growth, He plasma irradiation can be sorted in terms of homologous temperature, which is the temperature normalized to the melting point (T_s/T_m). Helium plasma irradiation to different metals shows that the fuzz growth occurs in the range of $0.25 < T_s/T_m < 0.6$.[21] The range of 850–1000 K in T_s for V corresponds to 0.39–0.46 in T_s/T_m, which is within the range described in ref. [21]. The high-temperature threshold is most likely below 0.6, and it can vary depending on the material. For example, it is ≈0.36 for Mo.[55]

It has been revealed that there are two major processes that counteract the fuzz growth: erosion by sputtering[56] and thermal annealing.[57] Fuzz formed partially at $T_s > 1050$ K, because the counter-growth process of thermal annealing dominated the growth process due to high temperatures. At $T_s > 1050$ K and $E_i > 90$ eV, it is likely that erosion by sputtering started to work in addition to the thermal annealing as the sputtering yield reached 10^{-2}.[58]

It is notable that the fuzz growth condition on thin film V is different from that previously reported on bulk V,[5] where fuzz was formed when $E_i > 115$ eV and $T_s > 1000$ K. One of the differences is attributed to the fact that the migration of He might be different between bulk V and thin film V. Thermal desorption spectra show that He desorbs at about 200 K lower temperature for a thin film compared to bulk (Figure S3, Supporting Information). During plasma exposure, He migration leads to the growth of He bubbles, which are thought to play an important role in the process of the formation of fuzz.[59] Hence, if the He migration is facilitated in thin films, for example, through lower density of the material, bubble formation and fuzz formation can start at milder conditions than in the bulk.

For PEC measurements, electrical contacts are needed. Therefore, V films were also deposited on Si substrates and exposed to He plasma. **Figure 3**a–c shows SEM micrographs of the V thin film prepared by radio frequency (RF) magnetron sputtering on a Si substrate and exposed to He plasma for 30, 60, and 120 min, respectively. It is found that a longer irradiation time of 120 min was required to form fuzz on the Si substrate compared to the SiO_2 substrate. Only protrusions were formed when the irradiation time was 30 or 60 min. The difference of nanofuzz formation on Si and SiO_2 substrates might be related to different thin film growth on Si compared to SiO_2 substrate,

© 2023 The Authors. Advanced Energy and Sustainability Research published by Wiley-VCH GmbH

26999412, 0, Downloaded from https://onlinelibrary.wiley.com/doi/10.1002/aesr.202200141 by Technical University Eindhoven, Wiley Online Library on [16/02/2023]. See the Terms and Conditions (https://onlinelibrary.wiley.com/terms-and-conditions) on Wiley Online Library for rules of use; OA articles are governed by the applicable Creative Commons License

26999412, 0, Downloaded from https://onlinelibrary.wiley.com/doi/10.1002/aesr.202200141 by Technical University Eindhoven, Wiley Online Library on [16/02/2023]. See the Terms and Conditions (https://onlinelibrary.wiley.com/terms-and-conditions) on Wiley Online Library for rules of use; OA articles are governed by the applicable Creative Commons License

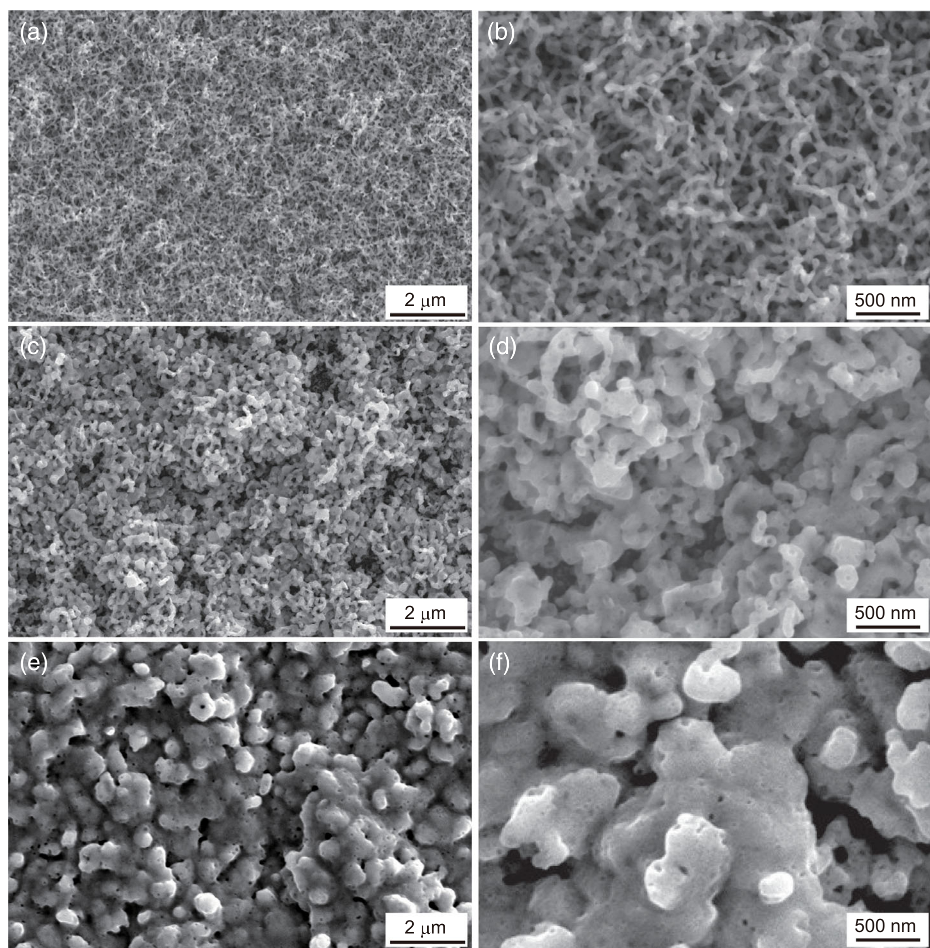

Figure 1. Scanning electron microscope (SEM) micrographs of V thin films exposed to He plasmas with SiO_2 substrates without additional calcination at different magnifications. The irradiation conditions (T_s, E_i, and Φ_{He}) are as follows: a,b) 970 K, 70 eV, and 5.4×10^{25} m^{-2} (fuzz), c,d) 1080 K, 70 eV, and 9.4×10^{25} m^{-2} (partially fuzz), and e,f) 1120 K, 95 eV, and 1.6×10^{26}m^{-2} (roughened).

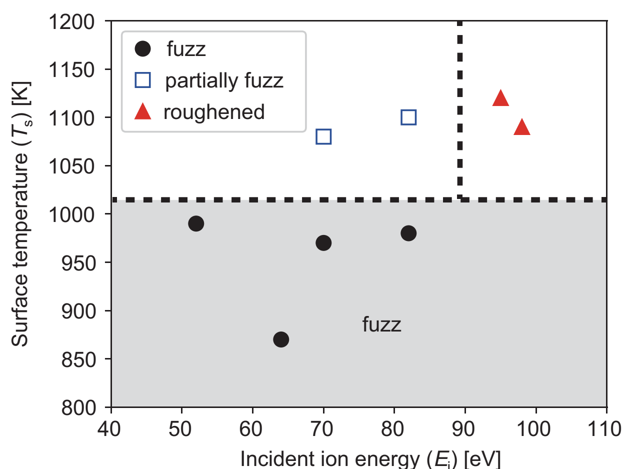

Figure 2. Summary of the morphology change of V thin film on SiO_2 substrates. (The lines are guide for the eye.)

which can result in differences in the density of the thin film; this will be studied in more detail in a follow-up study.

3. Structure and Surface Chemistry

The fabricated V thin films were oxidized in the furnace at 773 K for 30 min. Two different samples are compared here: a thin film without plasma irradiation (V_{flat}) and a nanostructured thin film with He plasma irradiation (V_{nano}). The irradiation condition of V_{nano} was as follows: $E_i = 70$ eV, $T_s = 970$ K, and $\Phi_{He} = 5.4 \times 10^{25}$ m^{-2}.

Figure 4 shows X-ray photoelectron spectroscopy (XPS) survey spectra of V_{flat} and V_{nano} after calcination. Vanadium, C, and O were the major signal on V_{flat}. It was found that Mo signals were seen on V_{nano} in addition to the peaks found on V_{flat}. **Figure 5**a shows the V 2p XPS spectra of V_{flat} and V_{nano}. The binding energy was calibrated with respect to the position of the O 1s spectrum in a manner similar to ref. [60]. The dotted lines in Figure 5a indicate the positions of V^{5+} (517.2 eV), V^{4+} (515.84 eV), and V^{3+} (515.29 eV).[61] For V_{flat}, a clear V^{5+} is formed, which means that V_2O_5 is formed on the surface. For V_{nano}, a broad tail in the lower-energy region is found, suggesting that lower oxidation states of V^{4+} and V^{3+} are mixed with V^{5+}. The peaks of V^{4+} and V^{3+} on V_{flat} are mixed and cannot be

© 2023 The Authors. Advanced Energy and Sustainability Research published by Wiley-VCH GmbH

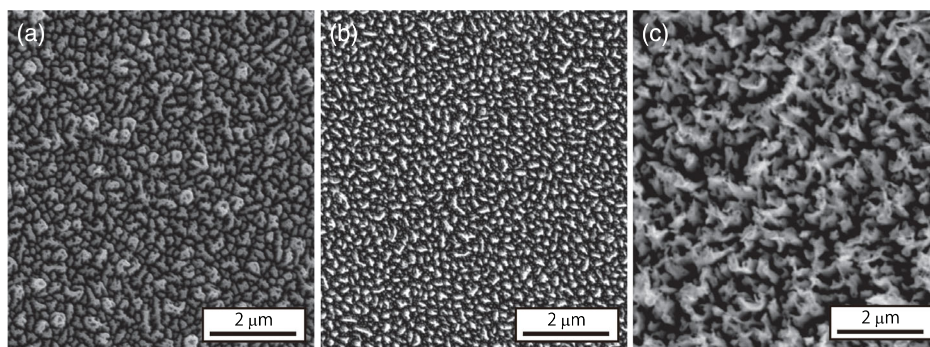

Figure 3. a–c) SEM micrographs of the V thin films (without calcination) prepared by RF magnetron sputtering on a Si substrate and exposed to the He plasma for 30, 60, and 120 min, respectively. The irradiation condition (T_s, E_i, and Φ_{He}) is as follows: (a) 960 K, 74 eV, and 3.4×10^{25} m^{-2}, (b) 940 K, 72 eV, and 6.1×10^{25} m^{-2}, and c) 960 K, 76 eV, and 1.3×10^{26} m^{-2}. (He irradiation with no additional calcination.)

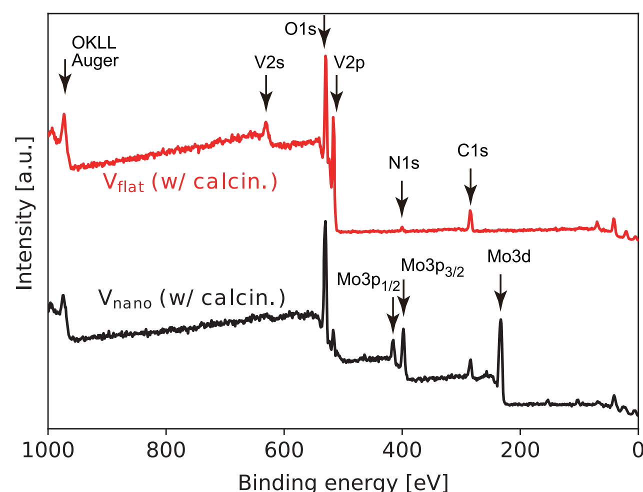

Figure 4. XPS survey spectra of V_{flat} and V_{nano} after calcination.

separated, and the fraction other than V^{5+} was 4.4%. Three peaks were separately identified on V_{nano}, and the fractions of V^{4+} and V^{3+} were obtained to be 17% and 14%, respectively. Hence, the fraction of lower-oxidation states increased on the sample with the plasma irradiation.

Figure 5b shows the O 1*s* XPS spectra of V_{flat} and V_{nano} before and after calcination. The peak at 530.0 eV is from the lattice of vanadium oxides, and another peak around 532 eV corresponds to hydroxyl (OH^-) or oxygen vacancies ($V_{\ddot{o}}$).[40,62] It was found that the peak at 532 eV is larger on V_{nano} than on V_{flat}. The fractions of $OH^-/V_{\ddot{o}}$ obtained from the fit with the double Gaussian function are 0.17 and 0.28 on V_{flat} and V_{nano}, respectively. The peak at 532 eV before calcination was larger than that after calcination and was 0.25 and 0.53 on V_{flat} and V_{nano}, respectively. It is seen that the calcination process decreased the fraction of the vacancy by 50–60%.

Figure 6 shows X-ray diffraction (XRD) patterns of V_{flat} and V_{nano}. A broad background centered around $2\theta = 22°$ is attributed to the signal from the SiO_2 substrate.[40] On V_{flat}, typical V_2O_5 peaks[16] are observed. On V_{nano}, peaks of other oxides, such as V_6O_{13}, V_2O_3, and VO_2, are identified next to V_2O_5. As was found in the XPS survey spectra (Figure 4), the peaks from MoO_3 are also included in the XRD pattern, suggesting that mixed layer of V and Mo oxides are formed. A broad peak around 20° from the SiO_2 substrate is clearly identified on V_{nano}. Because nanostructures form on the surface, the signal from the bulk Si is easier to detect. The oxidation states of V_2O_5, V_6O_{13}, and V_2O_3 are 5+, a mixture of 4+ and 5+, and 3+, respectively. Thus, the XRD results are consistent with the XPS spectra in Figure 5, where V_{nano} showed peaks from V^{3+} to V^{5+}, while V_{flat} showed only a clear V^{5+} peak.

4. Photoelectrochemistry

Figure 7a shows the photocurrent density on V_{flat} (black) and V_{nano} (red) as a function of the applied potential, ϕ_{RHE}, when the light is chopped at 1 Hz. The potential is scanned from low to high potential. For both samples, the photocurrent gradually increases, and the slope steepens from around the theoretical voltage for water-splitting of 1.23 V_{RHE}; the dark current stays constant. The current density of V_{nano} is found to be about twice as high as the current density of V_{flat} at 1.23 V_{RHE}. In the entire range of applied potential, the photocurrent of V_{nano} is significantly higher than that of V_{flat}. Figure 7b shows the current density at 1.23 V_{RHE} for unexposed samples with three different thin-film thicknesses (50, 100, 200 nm—green color) and for 200 nm thick samples which were plasma exposed for different times (30, 60, 120 min—blue color). It is found that the current density at 1.23 V_{RHE} is comparable for the three unexposed samples with different film thickness. Hence, the vanadium oxide film thickness has no significant impact on the current density at 1.23 V_{RHE}. After plasma exposure (blue color), the current density is significantly higher. In addition, it is increasing the longer the irradiation time. A 2.8-fold increase in current density is found for an irradiation time of 120 min. The increase in current density can be related to nanostructuring and/or chemical changes and will be discussed in more detail in Section 5.

Figure 8 shows a comparison of electrochemical impedance spectroscopy (EIS) analysis between V_{flat} and V_{nano} (with illumination). As shown in Figure 8a, the low-frequency arc in the Nyquist diagram is smaller for V_{nano}, suggesting that the

© 2023 The Authors. Advanced Energy and Sustainability Research published by Wiley-VCH GmbH

26999412, 0, Downloaded from https://onlinelibrary.wiley.com/doi/10.1002/aesr.202200141 by Technical University Eindhoven, Wiley Online Library on [16/02/2023]. See the Terms and Conditions (https://onlinelibrary.wiley.com/terms-and-conditions) on Wiley Online Library for rules of use; OA articles are governed by the applicable Creative Commons License

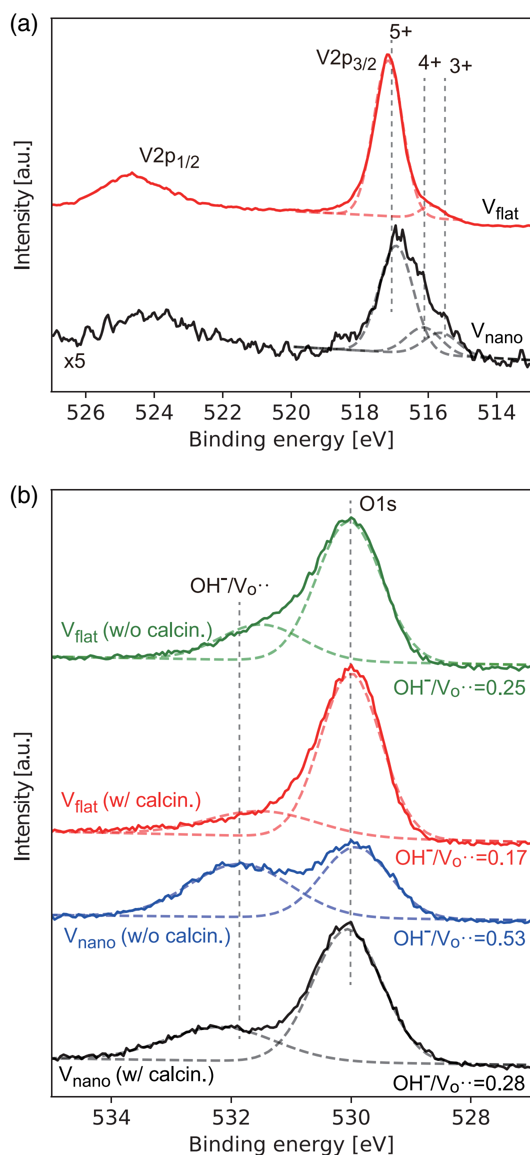

Figure 5. a) V 2*p* XPS spectra after calcination and b) O 1*s* XPS spectra before and after calcination of vanadium oxide samples (V_{flat} and V_{nano}).

charge-transfer resistance decreases by the plasma irradiation. The impedance data was fitted using an equivalent circuit shown in Figure 8b. The capacitance, C_{bulk}, and the charge-transfer resistance, R_{CT}, are plotted for V_{flat} and V_{nano} as a function of V_{RHE} in Figure 8c,d, respectively. Comparing V_{nano} to V_{flat}, it is seen that C_{bulk} increased by 30–40% (37% at maximum) and R_{CT} decreased by 25–35% (33% at maximum) due to plasma irradiation.

5. Discussion

The PEC performance was increased 2.8-fold by He plasma irradiation. Four factors can contribute to the increase in current density: 1) increase in the surface area due to the morphology change; 2) formation of composite structure with MoO_3; 3) changes of the oxidation state of vanadium; and 4) formation of oxygen vacancies. Each factor is discussed separately in the following:

Increase in surface area: although the surface area of V fuzzy samples has yet to be measured, the surface area of fuzzy W measured by the BET method deduced an order of magnitude increase due to morphology changes;[63] the surface area has increased to about 20 times when the fuzzy layer thickness is 1 μm on W. Similarly, the EIS of iron oxide (Fe_2O_3) thin films showed an increase in active surface area by the He plasma irradiation due to the formation of nanostructures.[38] However, the PEC performance does not necessarily increase monotonically with surface area. In nanostructured Fe_2O_3, the performance did not increase proportionally to the active surface area, and the presence of secondary elements and secondary iron oxide phases was assumed to be the cause.[38] Plasma exposure increases the active surface area. At the same time, it creates defects in the lattice, which can lead to a decrease in the performance. Hence, increase in surface area might not be proportional to increase in performance. This explains why the increase in performance in this study is less than expected from the micrographs. The increase in C_{bulk} in Figure 8c supports that the increase in the active surface area contributes to the increase in the PEC performance.

Formation of composite structure with MoO_3: additional secondary semiconductor to form a heterojunction photoelectrode is a popular way to enhance the photocatalytic activity as improving charge separation of formed electron–hole pairs.[64] A mechanism of an enhanced photocatalytic performance of V_2O_5/MoO_3 composite was discussed by Chuai et al.,[51] where photocatalytic activity for the degradation of methylene blue was significantly improved from 49.9% on pure V_2O_5 to 89.2% on V_2O_5/MoO_3 composite. Although the conduction band (CB) position of MoO_3 could be higher than that of V_2O_5, V-doped MoO_3 caused a lower CB position than that of V_2O_5 and allowed the photogenerated electrons formed on V_2O_5 to be injected into the CB of MoO_3. It was discussed that photoexcitation can occur both on V_2O_5 and MoO_3 and that the accumulation of photoexcited electrons and holes occurs on MoO_3 and V_2O_5, respectively, leading to the separation of electron–hole pairs and the reduction of electron–hole recombination. In the same manner, composite of V_2O_5/MoO_3 formed on V_{nano} could be contributed to the enhanced PEC performance as reducing the recombination of the photogenerated electron–hole pairs on the surface.

Changes of the oxidation state of vanadium: a broadening of V 2*p* spectra (Figure 5a) and changes in the XRD pattern (Figure 6) show that the formation of reduced oxides, such as V_6O_{13} and V_2O_3, are mixed with V_2O_5 on V_{nano}. Such mixed peaks of multiple vanadium oxides have been reported in studies using other synthesis methods.[16,65] In ref., [16] experiments on hydrogen production using visible light showed that the accumulative amount of hydrogen production was higher for V_6O_{13} than for V_2O_5.

Formation of oxygen vacancy: as shown in Figure 5b, the fraction of $OH^-/V_{\ddot{o}}$ increased by 64%, from 0.17 to 0.28 for V_{nano}. Oxygen vacancies are known to be formed by annealing in oxygen-depleted environments, exposure to energetic particles, ion

© 2023 The Authors. Advanced Energy and Sustainability Research published by Wiley-VCH GmbH

26999412, 0, Downloaded from https://onlinelibrary.wiley.com/doi/10.1002/aesr.202200141 by Technical University Eindhoven, Wiley Online Library on [16/02/2023]. See the Terms and Conditions (https://onlinelibrary.wiley.com/terms-and-conditions) on Wiley Online Library for rules of use; OA articles are governed by the applicable Creative Commons License

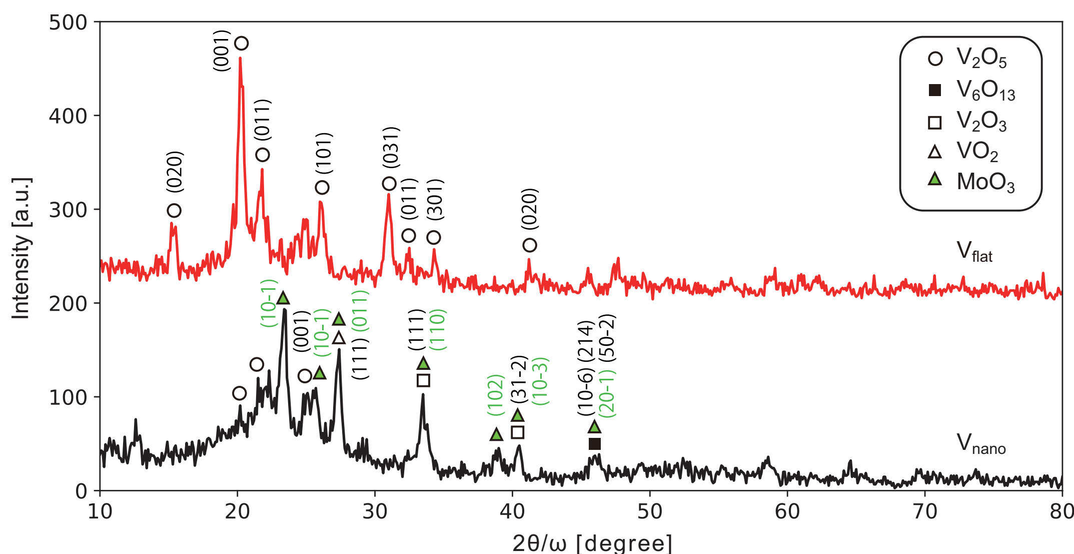

Figure 6. XRD patterns of V_{flat} (red) and V_{nano} (black) after calcination. An inorganic materials database system, AtomWork,[72] was used to assign the diffraction peaks. (The following references are used for each element: V_2O_5[73–78] $VO_2V_2O_3V_6O_{13}MoO_3$.)

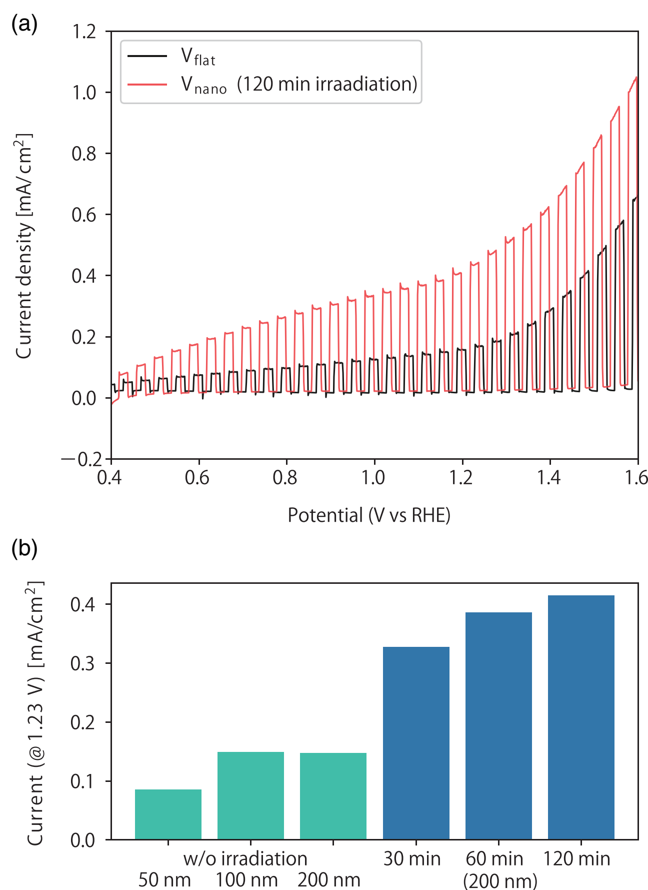

Figure 7. a) Photocurrent density on V_{flat} and V_{nano} as a function of ϕ_{RHE} with chopped light at 1 Hz and b) the photocurrent density of six samples at different plasma exposure times including the one without irradiation. A 0.1 M KOH solution with a pH of 13.0 was used as the electrolyte. All the samples were calcinated in air at 773 K for 30 min.

doping, and also He plasma irradiation, and this plays an important role in the performance of photocatalysts.[62] Vacancy engineering exists in other fields as well.[66] For TiO_2 and WO_3, He plasma irradiation increases oxygen vacancy, and the contribution to the improvement of photocatalytic and PEC performance has been discussed.[40,67] On V oxides, the role of the oxygen vacancies in enhancing the diffusion of ions, such as Zn and Li ions, has been investigated for battery applications.[68,69] There are no reports about the effect of oxygen vacancies on the photocatalytic or PEC performance of vanadium oxides.

In addition to the fact that the increase in surface area led to an increase in C_{bulk}, a mixture of the aforementioned three factors (2)–(4), that is, composite formation, different oxidation states, and oxygen vacancies, is believed to reduce R_{CT} and resulted in an improvement in PEC performance.

6. Conclusions

In this study, He plasma treatment was performed on V thin films, which were deposited on Si and on SiO_2 substrates by sputtering. Helium plasma irradiation resulted in various morphology changes depending on T_s and E_i while inducing auxiliary Mo deposition from the sample holder. Fuzz growth occurred when T_s was in the range of 850–1000 K. Compared to the previous study, where He plasma treatment was performed on bulk V, the required T_s and E_i for nanostructure formation were higher than in this study. This was likely caused by the fact that He atoms move more easily at low temperatures in the thin film.

Surface characterization by XPS/XRD and PEC measurements were performed using the thin films oxidized in a furnace at 773 K. The photocurrent increased with increasing the irradiation time, and it became 2.2 (at 30 min) to 2.8 (at 120 min) times higher than that without He plasma treatment. The EIS analysis

© 2023 The Authors. Advanced Energy and Sustainability Research published by Wiley-VCH GmbH

26999412, 0, Downloaded from https://onlinelibrary.wiley.com/doi/10.1002/aesr.202200141 by Technical University Eindhoven, Wiley Online Library on [16/02/2023]. See the Terms and Conditions (https://onlinelibrary.wiley.com/terms-and-conditions) on Wiley Online Library for rules of use; OA articles are governed by the applicable Creative Commons License

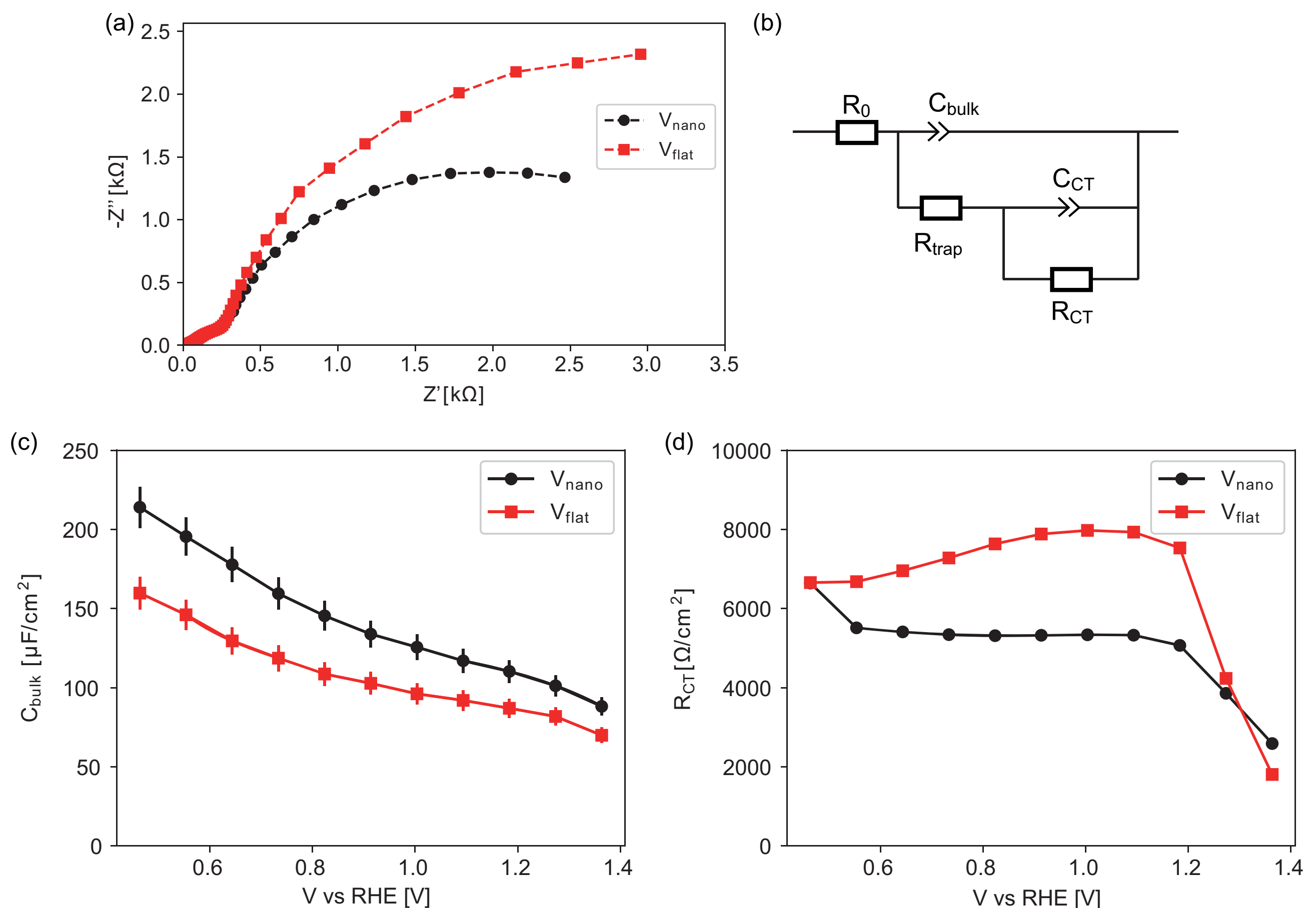

Figure 8. a) Nyquist plot at 1.2 V_{RHE} for V_{flat} and V_{nano}, b) equivalent circuit model used for analyzing the electrochemical impedance spectroscopy (EIS) data, and V_{RHE} dependences of c) bulk capacitance (C_{bulk}) and d) charge-transfer resistance (R_{CT}) for V_{flat} and V_{nano}.

suggested that both the increase in C_{bulk} and the decrease in R_{CT} contributed to the enhanced PEC performance. In other words, in addition to the increase in surface area due to the morphology change, the water oxidation kinetics was also improved. The formation of V/Mo oxide composites, the formation of different oxidation states, such as V_6O_{13}, which are probably more active than V_2O_5,[16] and the formation of oxygen vacancies are the potential factors.

This work shows that the use of He plasma offers different paths for improving the performance of electrodes for PEC water-splitting. It has a potential to control surface morphology, form composite, and induce vacancies in a one-step process of He plasma irradiation. In the future, an additional sputtering source to control the deposition rate of Mo will be introduced, such as demonstrated previously,[70] it will be a versatile method with a better controllability.

7. Experimental Section

Sample Fabrication: A linear plasma device, the details of which are shown elsewhere,[71] and a radio frequency magnetron sputtering device (HSR-522, SHIMADZU) were used to form V thin films (typically, 200 nm in thickness) in an argon atmosphere. Fused silica glass (SiO_2) was used for the substrate to perform systematic plasma irradiation experiments and surface characterization, and a conductive silicon (Si) substrate was used for PEC measurements. The surface temperature, which was measured by a thermocouple, was 320 K during deposition.

The V thin films were exposed to He plasmas in a linear plasma device named NAGDIS-II,[33] where high-density He plasma ($10^{18}-10^{19} m^{-3}$) can be produced in a steady state. The substrate was installed in a water-cooled sample holder, which was biased negatively to control the incident ion energy, E_i. The incident ion energy was determined from the difference between the potential of the sample and the plasma potential, which was measured by an electrostatic probe. The ion flux was also measured by the electrostatic probe. The surface temperature, T_s, was measured using a thermopyrometer (KTL-PRO, LEC Co., Ltd.) at the wavelength of $\approx$ 1.6 μm.

The prepared V thin films were oxidized in air using a muffle furnace (FO100, Yamato Scientific Co., Ltd.) at 773 K for 30 min. In addition to the surface observation by field-emission scanning electron microscope (FE-SEM) (Hitachi, S4300), XRD (Rigaku, ATX-G) and XPS (ESCALAB250Xi, Thermo Scientific) were used for the surface analysis.

PEC: The PEC experiments were carried out in a standard three-electrode system using a potentiostat (SP-150, BioLogical) with the sample as the working electrode (WE), Pt wire as the counter electrode, and an Ag/AgCl/sat KCl electrode as the reference electrode (RE). A 0.1 M KOH solution with a pH of 13.0 was used as the electrolyte. In the three-electrode system, the bias voltage ($\phi_{Ag/AgCl}$) applied between WE and RE at the potentiostat is given as the potential versus a reversible hydrogen electrode (RHE) by the following relation.

© 2023 The Authors. Advanced Energy and Sustainability Research published by Wiley-VCH GmbH

26999412, 0, Downloaded from https://onlinelibrary.wiley.com/doi/10.1002/aesr.202200141 by Technical University Eindhoven, Wiley Online Library on [16/02/2023]. See the Terms and Conditions (https://onlinelibrary.wiley.com/terms-and-conditions) on Wiley Online Library for rules of use; OA articles are governed by the applicable Creative Commons License

$$\phi_{RHE} = \phi_{Ag/AgCl} + \phi^{o}_{Ag/AgCl} + 0.059 \times pH \tag{1}$$

where $\phi_{Ag/AgCl}$ is the experimentally measured WE potential and $\phi^{o}_{Ag/AgCl}$ is 0.197 V at 25 °C. Because the pH is 13.0

$$\phi_{RHE} = \phi_{Ag/AgCl} + 0.964 \tag{2}$$

A 300 W xenon lamp was used as the light source, and a photocurrent density curve was obtained by applying a potential of −1.5–+1.5 V to the Ag/AgCl electrode at a scan rate of 10 mV s^{-1} while chopping the light using a mechanical shutter at a frequency of 0.5 s^{-1}.

Supporting Information

Supporting Information is available from the Wiley Online Library or from the author.

Acknowledgements

This work was supported in part by a Grant-in-Aid for Scientific Research (Grant nos. 19H01874 and 21K18617), and Fund for the Promotion of Joint International Research (Grant nos. 17KK0132 and 21KK0048) from the Japan Society for the Promotion of Science (JSPS) and JSPS Bilateral Joint Research Projects.

Conflict of Interest

The authors declare no conflict of interest.

Data Availability Statement

The data that support the findings of this study are available from the corresponding author upon reasonable request.

Keywords

fuzz, helium plasma, nanostructures, photoelectrochemical performances, vanadium

Received: September 27, 2022
Revised: January 3, 2023
Published online:

[1] A.-M. Cao, J.-S. Hu, H.-P. Liang, L.-J. Wan, *Angew. Chem., Int. Ed.* **2005**, *44*, 4391.
[2] Q. Wei, R. H. DeBlock, D. M. Butts, C. Choi, B. Dunn, *Energy Environ. Mater.* **2020**, *3*, 221.
[3] Q. Van Overmeere, S. Ramanathan, *Electrochim. Acta* **2014**, *150*, 83.
[4] T. K. Le, M. Kang, V. T. Tran, S. W. Kim, *Mater. Sci. Semicond. Process.* **2019**, *100*, 159.
[5] S. Kajita, T. Yoshida, N. Ohno, Y. Ichino, N. Yoshida, *J. Phys. D: Appl. Phys.* **2018**, *51*, 215201.
[6] R. Alrammouz, M. Lazerges, J. Pironon, I. Bin Taher, A. Randi, Y. Halfaya, S. Gautier, *Sens. Actuators, A* **2021**, *332*, 113179.
[7] M. Liu, B. Su, Y. Tang, X. Jiang, A. Yu, *Adv. Mater.* **2017**, *7*, 1700885.
[8] Y. Wang, G. Cao, *Chem. Mater.* **2006**, *18*, 2787.
[9] S. Beke, S. Giorgio, L. Korosi, L. Nanai, W. Marine, *Thin Solid Films* **2008**, *516*, 4659.
[10] X. Wang, H. Li, Y. Fei, X. Wang, Y. Xiong, Y. Nie, K. Feng, *Appl. Surf. Sci.* **2001**, *177*, 8.
[11] M. E. Warwick, R. Binions, *J. Solid State Chem.* **2014**, *214*, 53.
[12] M. Seman, J. Marino, W. Yang, C. A. Wolden, *J. Non-Cryst. Solids* **2005**, *351*, 1987.
[13] O. Monfort, T. Roch, L. Satrapinskyy, M. Gregor, T. Plecenik, A. Plecenik, G. Plesch, *Appl. Surf. Sci.* **2014**, *322*, 21.
[14] V. Vivier, J. Farcy, J.-P. Pereira-Ramos, *Electrochim. Acta* **1998**, *44*, 831.
[15] D. Vasanth Raj, N. Ponpandian, D. Mangalaraj, C. Viswanathan, *Mater. Sci. Semicond. Process.* **2013**, *16*, 256.
[16] T. F.-R. Shen, M.-H. Lai, T. C.-K. Yang, I.-P. Fu, N.-Y. Liang, W.-T. Chen, *J. Taiwan Inst. Chem. Eng.* **2012**, *43*, 95.
[17] K. Zhu, Y. Meng, H. Qiu, Y. Gao, C. Wang, F. Du, Y. Wei, G. Chen, C. Wang, G. Chen, *J. Alloys Compd.* **2015**, *650*, 370.
[18] L. Mai, L. Xu, C. Han, X. Xu, Y. Luo, S. Zhao, Y. Zhao, *Nano Lett.* **2010**, *10*, 4750, pMID: 20954742.
[19] D. Zintu, G. Tosone, A. Mercuri, *Infrared Phys. Technol.* **2002**, *43*, 245.
[20] S. Takamura, N. Ohno, D. Nishijima, S. Kajita, *Plasma Fusion Res.* **2006**, *1*, 051.
[21] S. Kajita, T. Nojima, Y. Tomita, N. Ohno, H. Tanaka, N. Yoshida, M. Yajima, T. Akiyama, M. Tokitani, T. Yagi, *Surf. Coat. Technol.* **2018**, *340*, 86.
[22] J. Tripathi, T. Novakowski, A. Hassanein, *Appl. Surf. Sci.* **2016**, *378*, 63.
[23] Y. Ueda, N. Yamashita, K. Omori, H. Lee, K. Ibano, A. Ito, *J. Nucl. Mater.* **2018**, *511*, 605.
[24] K. Omori, A. M. Ito, K. Shiga, N. Yamashita, K. Ibano, H. T. Lee, Y. Ueda, *J. Appl. Phys.* **2017**, *121*, 155301.
[25] S. Kajita, A. M. Ito, K. Ibano, *J. Appl. Phys.* **2022**, *132*, 181101.
[26] S. Kajita, N. Yoshida, N. Ohno, Y. Tsuji, *New J. Phys.* **2015**, *17*, 043038.
[27] S. Kajita, T. Nojima, T. Okuyama, Y. Yamamoto, N. Yoshida, N. Ohno, *Acta Mater.* **2019**, *181*, 342.
[28] Y. V. Martynenko, M. Y. Nagel, *Plasma Phys. Rep.* **2012**, *38*, 996.
[29] A. Ito, A. Takayama, Y. Oda, T. Tamura, R. Kobayashi, T. Hattori, S. Ogata, N. Ohno, S. Kajita, M. Yajima, Y. Noiri, Y. Yoshimoto, S. Saito, S. Takamura, T. Murashima, M. Miyamoto, H. Nakamura, *Nucl. Fusion* **2015**, *55*, 073013.
[30] K. D. Hammond, S. Blondel, L. Hu, D. Maroudas, B. D. Wirth, *Acta Mater.* **2018**, *144*, 561.
[31] K. Ibano, Y. Kimura, T. Sugahara, H. T. Lee, Y. Ueda, *Jpn. J. Appl. Phys.* **2018**, *57*, 040316.
[32] Y. Kimura, K. Ibano, K. Uehata, I. Hirai, H. Tae Lee, Y. Ueda, *Appl. Surf. Sci.* **2020**, *532*, 147274.
[33] S. Kajita, T. Yoshida, D. Kitaoka, R. Etoh, M. Yajima, N. Ohno, H. Yoshida, N. Yoshida, Y. Terao, *J. Appl. Phys.* **2013**, *113*, 134301.
[34] M. de Respinis, G. De Temmerman, I. Tanyeli, M. C. van de Sanden, R. P. Doerner, M. J. Baldwin, R. van de Krol, *ACS Appl. Mater. Interfaces* **2013**, *5*, 7621.
[35] K. Komori, T. Yoshida, T. Nomoto, M. Yamamoto, C. Tsukada, S. Yagi, M. Yajima, S. Kajita, N. Ohno, *Nucl. Instrum. Methods Phys. Res., Sect. B* **2015**, *365*, 35.
[36] S. Feng, S. Kajita, M. Higashi, A. Bieberle-Hutter, T. Yoshida, N. Ohno, *Appl. Surf. Sci.* **2022**, *580*, 151979.
[37] A. Bieberle-Hütter, I. Tanyeli, R. Lavrijsen, B. Koopmans, R. Sinha, M. van de Sanden, *Thin Solid Films* **2017**, *631*, 50.
[38] R. Sinha, I. Tanyeli, R. Lavrijsen, M. van de Sanden, A. Bieberle-Hütter, *Electrochim. Acta* **2017**, *258*, 709.
[39] Y. Tomita, S. Kajita, E. Yasunaga, T. Yoshida, N. Ohno, H. Tanaka, *Jpn. J. Appl. Phys.* **2019**, *58*, SE SEEG01.
[40] S. Kajita, K. Miyaguchi, H. Tanaka, E. Yasunaga, T. Yoshida, N. Ohno, *J. Photochem. Photobiol., A* **2021**, *418*, 113420.
[41] Y. Zhao, S. Balasubramanyam, R. Sinha, R. Lavrijsen, M. A. Verheijen, A. Bol, A. Bieberle-Hutter, *ACS Appl. Energy Mater.* **2018**, *1*, 5887.
[42] S. Feng, S. Kajita, Y. Tomita, T. Yoshida, N. Ohno, *Jpn. J. Appl. Phys.* **2020**, *59*, SA SAAB04.

© 2023 The Authors. Advanced Energy and Sustainability Research published by Wiley-VCH GmbH

26999412, 0, Downloaded from https://onlinelibrary.wiley.com/doi/10.1002/aesr.202200141 by Technical University Eindhoven, Wiley Online Library on [16/02/2023]. See the Terms and Conditions (https://onlinelibrary.wiley.com/terms-and-conditions) on Wiley Online Library for rules of use; OA articles are governed by the applicable Creative Commons License

[43] S. Feng, S. Kajita, M. Tokitani, D. Nagata, N. Ohno, *Plasma Sci. Technol.* **2022**, https://doi.org/10.1088/2058-6272/ac9f2d.
[44] A. B. Djurisic, Y. H. Leung, A. M. Ching Ng, *Mater. Horiz.* **2014**, *1*, 400.
[45] N. Zhang, C. Gao, Y. Xiong, *J. Energy Chem.* **2019**, *37*, 43.
[46] S. Rehman, R. Ullah, A. Butt, N. Gohar, *J. Hazard. Mater.* **2009**, *170*, 560.
[47] A. Kudo, Y. Miseki, *Chem. Soc. Rev.* **2009**, *38*, 253.
[48] V. H. Nguyen, L. G. Bach, Q. T. P. Bui, T. D. Nguyen, D.-V. N. Vo, H. T. Vu, S. T. Do, *J. Environ. Chem. Eng.* **2018**, *6*, 7434.
[49] M. Arunachalam, K.-S. Ahn, S. H. Kang, *Int. J. Hydrogen Energy* **2019**, *44*, 4656.
[50] C. S. Yaw, Q. Ruan, J. Tang, A. K. Soh, M. N. Chong, *Chem. Eng. J.* **2019**, *364*, 177.
[51] H. Chuai, D. Zhou, X. Zhu, Z. Li, W. Huang, *Chin. J. Catal.* **2015**, *36*, 2194.
[52] G. Mitran, F. Neatu, O. D. Pavel, M. M. Trandafir, M. Florea, *Materials* **2019**, *12*, 5.
[53] C. Patil, P. Jadhav, N. Tarwal, H. Deshmukh, M. Karanjkar, P. Patil, *Mater. Chem. Phys.* **2011**, *126*, 711.
[54] T. Petty, M. Baldwin, M. Hasan, R. Doerner, J. Bradley, *Nucl. Fusion* **2015**, *55*, 093033.
[55] S. Takamura, *Plasma Fusion Res.* **2014**, *9*, 1405131.
[56] R. Doerner, M. Baldwin, P. Stangeby, *Nucl. Fusion* **2011**, *51*, 043001.
[57] S. Kajita, N. Yoshida, R. Yoshihara, N. Ohno, T. Yokochi, M. Tokitani, S. Takamura, *J. Nucl. Mater.* **2012**, *421*, 22.
[58] N. Matsunami, Y. Yamamura, Y. Itikawa, N. Itoh, Y. Kazumata, S. Miyagawa, K. Morita, R. Shimizu, H. Tawara, *At. Data Nucl. Data Tables* **1984**, *31*, 1.
[59] S. Kajita, N. Yoshida, R. Yoshihara, N. Ohno, M. Yamagiwa, *J. Nucl. Mater.* **2011**, *418*, 152.
[60] J. Mendialdua, R. Casanova, Y. Barbaux, *J. Electron. Spectrosc. Relat. Phenom.* **1995**, *71*, 249.
[61] G. Silversmit, D. Depla, H. Poelman, G. B. Marin, R. De Gryse, *J. Electron. Spectrosc. Relat. Phenom.* **2004**, *135*, 167.
[62] X. Pan, M.-Q. Yang, X. Fu, N. Zhang, Y.-J. Xu, *Nanoscale* **2013**, *5*, 3601.
[63] M. Yajima, Y. Hatano, S. Kajita, J. Shi, M. Hara, N. Ohno, *J. Nucl. Mater.* **2013**, *438*, S1142.
[64] S. J. A. Moniz, S. A. Shevlin, D. J. Martin, Z.-X. Guo, J. Tang, *Energy Environ. Sci.* **2015**, *8*, 731.
[65] P. Phoempoon, L. Sikong, *Sci. World J.* **2014**, *2014*, 841418.
[66] M. Ai, J.-W. Zhang, Y.-W. Wu, L. Pan, C. Shi, J.-J. Zou, *Chem. Asian J.* **2020**, *15*, 3599.
[67] S. Feng, S. Kajita, T. Yoshida, N. Ohno, D. Nagata, M. Tokitani, *Mater. Res. Express* **2020**, *7*, 075007.
[68] D. Zhao, Q. Zhu, X. Li, M. Dun, Y. Wang, X. Huang, *Batteries Supercaps* **2022**, *5*, e202100341.
[69] X. Peng, X. Zhang, L. Wang, L. Hu, S. H.-S. Cheng, C. Huang, B. Gao, F. Ma, K. Huo, P. K. Chu, *Adv. Funct. Mater.* **2016**, *26*, 784.
[70] Q. Shi, S. Kajita, S. Feng, N. Ohno, *J. Phys. D: Appl. Phys.* **2021**, *54*, 405202.
[71] K. Miyaguchi, S. Kajita, H. Tanaka, N. Ohno, *Jpn. J. Appl. Phys.* **2021**, *60*, 038004.
[72] Y. Xu, M. Yamazaki, P. Villars, *Japanese Journal of Applied Physics* **2011**, *50*, 11RH02.
[73] V. Voikov, G. Zakharova, M. Kuznetsov, *Russ. J. Inorg. Chem.* **1994**, *39*, 1808.
[74] J. Ketelaar, *Nature* **1936**, *137*, 316.
[75] M. Ghedira, H. Vincent, M. Marezio, J. Launay, *J. Solid State Chem.* **1977**, *22*, 423.
[76] P. D. Dernier, M. Marezio, *Phys. Rev. B* **1970**, *2*, 3771.
[77] I. Kawada, M. Ishii, M. Saeki, N. Kimizuka, M. Nakano-Onoda, K. Kato, *Acta Crystallogr., Sect. B: Struct. Crystallogr. Cryst. Chem.* **1978**, *34*, 1037.
[78] E. McCarron, J. Calabrese, *J. Solid State Chem.* **1991**, *91*, 121.

© 2023 The Authors. Advanced Energy and Sustainability Research published by Wiley-VCH GmbH

26999412, 0, Downloaded from https://onlinelibrary.wiley.com/doi/10.1002/aesr.202200141 by Technical University Eindhoven, Wiley Online Library on [16/02/2023]. See the Terms and Conditions (https://onlinelibrary.wiley.com/terms-and-conditions) on Wiley Online Library for rules of use; OA articles are governed by the applicable Creative Commons License